Supplementary Materials for

Electrochemical Synthesis of Au@Semiconductor Core-Shell Nanocrystals Guided by Single Particle Plasmonic Imaging

Hui Wang, ‡ Wei Zhao, ‡ Cong-Hui Xu,* Hong-Yuan Chen, Jing-Juan Xu*

State Key Laboratory of Analytical Chemistry for Life Science and Collaborative Innovation Center of Chemistry for Life Sciences, School of Chemistry and Chemical Engineering, Nanjing University, Nanjing 210023, China.

*Corresponding authors. Tel/fax: +86-25-89687294. E-mail: chxu@nju.edu.cn, xujj@nju.edu.cn

‡ These authors contributed equally to the work.

Table of contents

S1. Theoretical description of the LSPR peak position of Au@SC core shell structure.

For a core-shell nanostructure, the peak position of the surface plasmon could be estimated using equation 1.[1]

$$\lambda_{LSPR} = \lambda_p \left[12.2 + 2n_{water}^{2} + \frac{2g\left(n_{shell}^{2} - n_{water}^{2}\right)}{3} \right]^{\frac{1}{2}} \quad (1)$$

Where g is the volume fraction of the shell, n is the refractive index of the material at the wavelength of measurement, and λ_p is the bulk plasma wavelength of Au. For CdS with refractive index (n =2.5) greater than that of water (n =1.33), the LSPR peak shifts toward higher wavelengths with increase in g value. In addition, the absorption and scattering color change could be used to monitor the kinetics of surface nucleation and growth.

S2. DFM, SEM and TEM characterization of 80 nm Au coated with CdS shell.

We enlarged the size of Au NPs to 80 nm, the growth of shell was monitored using DFM and spectrometry in real time. As shown in Figure S1, 80 nm AuNP scattered dark greenyellow spot with λ_{max} centered at 580 nm according to the Lorentz fit. True-color digital camera and electrochemical workstation were triggered simultaneously via digital generator to monitor the synthesis of core-shell nanostructure in real-time. Under potential of -0.8 V (*vs.* Pt quasi-reference), the initial greenyellow spot turned brighter and generally changed to orange and red as time elapsed (Figure S1c). The scattering band was recorded every minute. In 9 min, the scattering peak shifted from 580 nm to 640 nm with significant intensity increase of 3.64-fold compared to the initial waveform. Meanwhile, the LSPR properties of Au@CdS with different shell thickness were analyzed using FDTD method, with a total field scattered-field source, theoretical simulation shows obvious scattering peak red-shift from 571.812 nm to 625.503 nm (Figure S2b) with 10 nm shell thickness increment, which exhibited the same trend with experimental results. The shell thickness varied from 5 ± 2 nm, 10 ± 2 nm, 15 ± 2 nm and 20 ± 2 nm corresponding to the electrodeposition time of 4, 8, 12 and 16 min. The shell was getting more uniform along with increasing deposition time. To further characterize the obtained core-shell structure, the in-situ formed Au@CdS NPs were separated from ITO substrate using ultrasound. Figure S2 show the typical TEM

images of the composite nanocrystals. The apparent contrast between the inner core and the outer shell can be seen with clear M/SC interface.

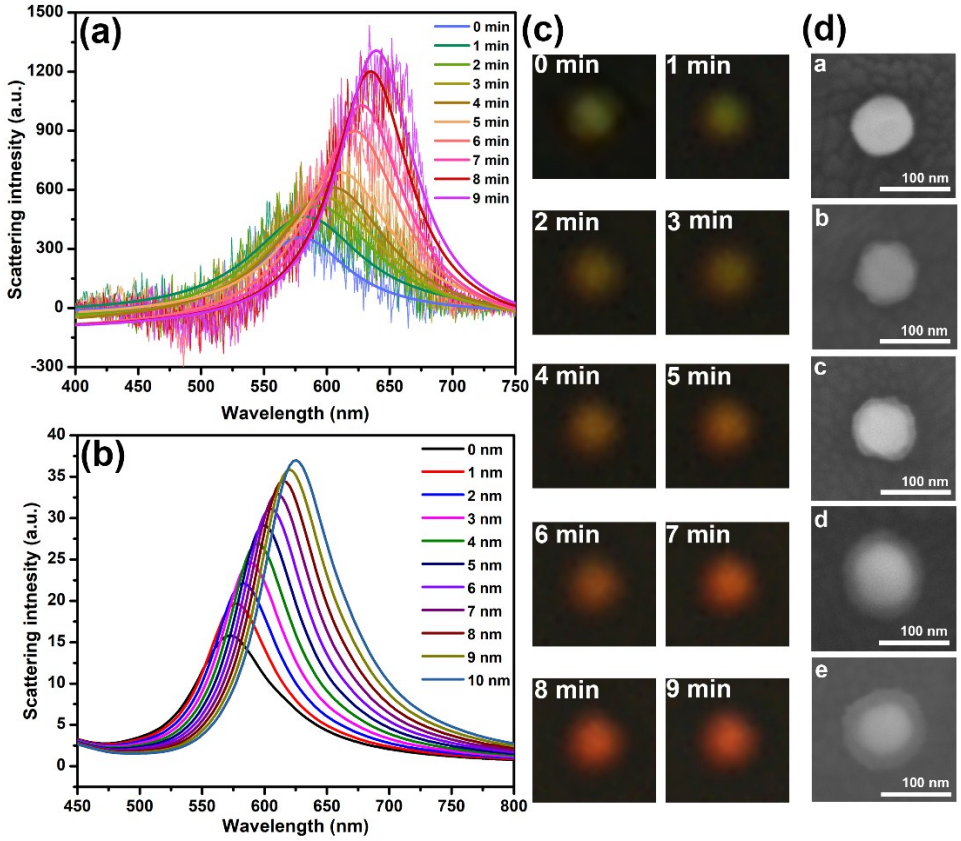

Figure S1. (a) Scattering spectra and Lorentz fit of an AuNP randomly selected during the electrochemical growth of CdS shell. (b) Simulation results of scattering spectra response of Au@CdS with different shell thickness. (c) Dark-field images of a single particle during the electrochemical growth of shell. (d) SEM images of 80 nm AuNP modified on ITO which undergoes different deposition time. a: 0 min, b: 4 min, c: 8 min, d: 12 min, e: 16 min.

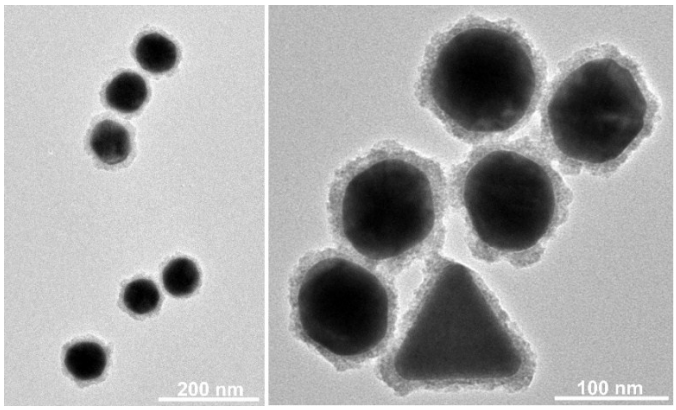

Figure S2. TEM images of 80 nm Au coated with CdS shell.

S3. Correlation of LSPR spectral shift with the shell thickness of Au@CdS NPs.

The correlation of shell thickness measured from SEM and TEM images with spectral shifts were estimated and shown in Figure S3. Mie theory indicated that the LSPR wavelength shifts exhibited an exponential relationship with shell thickness. In this work, $\Delta\lambda_{max}$ obtained from FDTD simulation, as well as the measured $\Delta\lambda_{max}$ from scattering spectra exhibited well exponential fits with shell thickness. Further, we also correlated the shell thickness with color change (ΔR/G), and presented the results in Figure 3c.

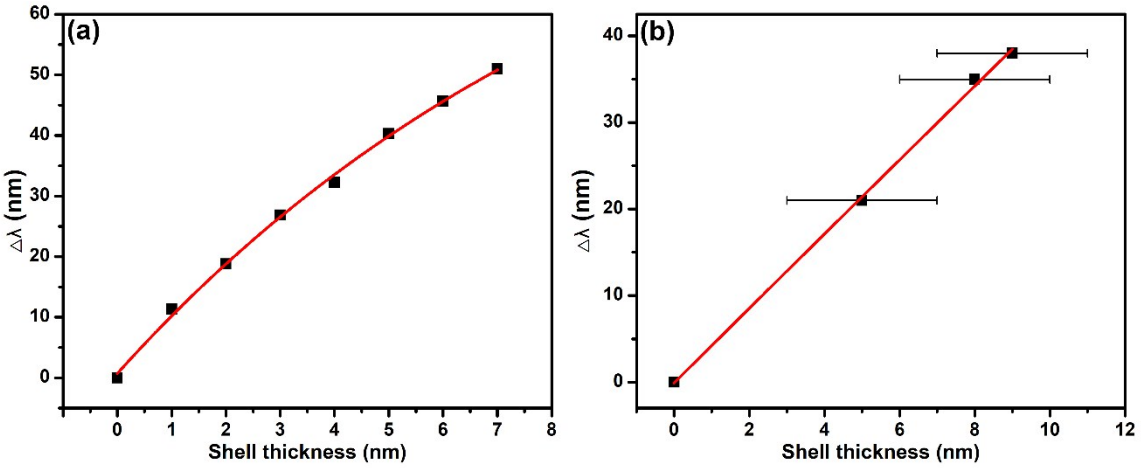

Figure S3. (a) The shell thickness dependence upon the simulated LSPR spectral shift by FDTD, the data were fit to a line with the equation y=99.65-98.94exp(-0.1x). (b) The estimated average shell thickness dependence upon the LSPR spectral shift, the data were fit to a line with the equation y=2822-2822exp(-0.0015x).

S4. TEM characterization of 40 nm Au@CdS NPs.

The in-situ synthesized Au@CdS NPs could be detached from ITO substrates via ultrasonic treatment. Characterized by TEM in Figure S4, it shows that the core-shell NPs have good homogeneity, which confirmed the estimation from plasmonic response to the CdS shell growth. The measured thickness was 5 ± 2 nm with the electrochemical deposition time of 3 min in Figure S5, which is similar to the value estimated from SEM images. HR-TEM images in Figure S6 exhibit that the d-spacing of 0.336 nm and 0.353 nm for the CdS shell is in agreement with the value for the hexagonal CdS(002) and CdS(100) plane. The enlarged HR-TEM image shown in Figure S6 indicate that no epitaxial relationship between

Au and CdS, the lattice mismatch is about 32.86% and 30.65% according to the measured lattice spacing in FigureS6a and S6b.

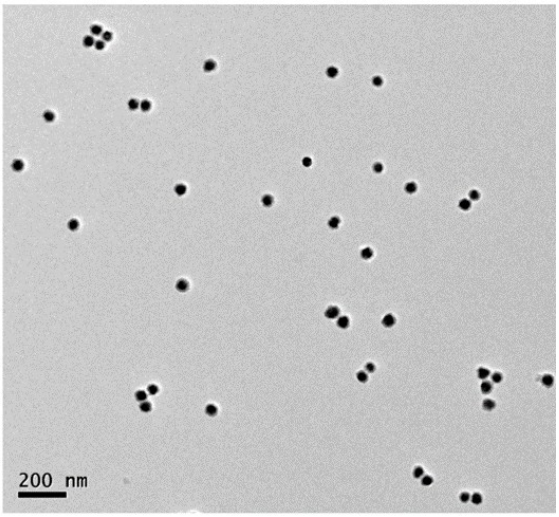

Figure S4. TEM images of electrochemical synthesized Au@CdS NPs with deposition time of 5 min.

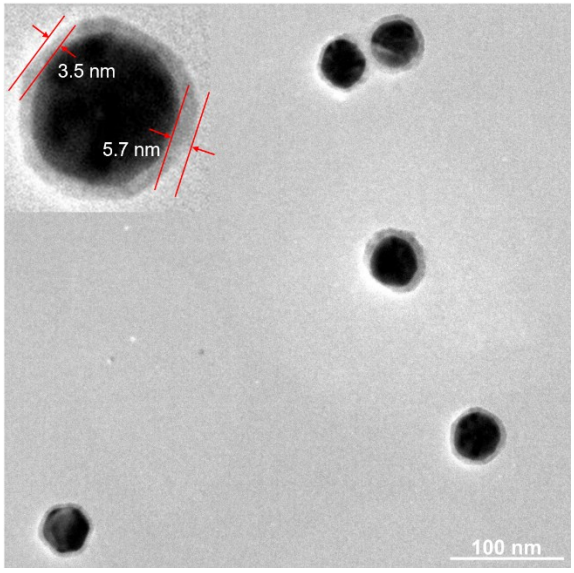

Figure S5. TEM images of electrochemical synthesized Au@CdS NPs with deposition time of 3 min.

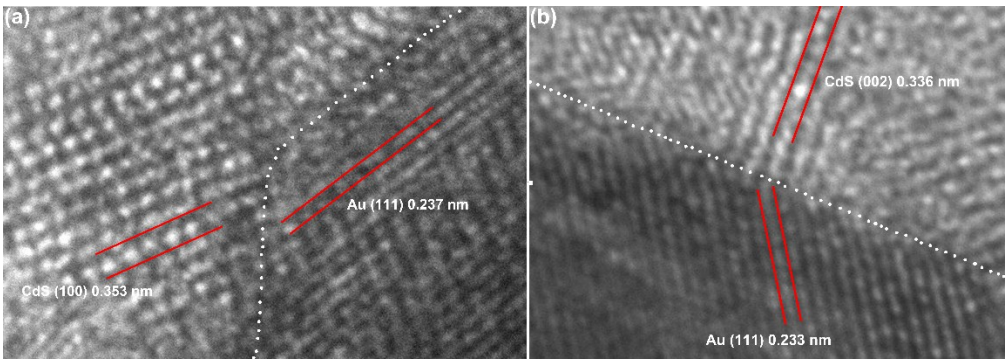

Figure S6. Enlarged HR-TEM image taken at the interface of Au and CdS regions.

S5. XRD measurements of Au@CdS, Au@ZnS and Au@CdSe NPs.

The X-ray diffraction (XRD) patterns of Au@CdS, Au@ZnS and Au@CdSe NPs are shown in Figure S7. As indicated in figure S7a, the peak at 28.3 (2θ) corresponds to the (101) diffraction planes of hexagonal CdS. For ZnS, the peaks at 28.7 (2θ), 30.5 (2θ) and 34.5 (2θ) correspond to the (103), (104) and (106) diffraction planes of wurtzite ZnS (Figure S7b). For Au@CdSe, it indicates that the peaks at 23.6 (2θ), 25.8 (2θ) and 35.3 (2θ) correspond to the (100), (002) and (102) diffraction planes (Figure S7c). Further, peaks at 38.2 (2θ), 44.5 (2θ), 64.6 (2θ) and 77.6 (2θ) correspond to the (111), (200), (220) and (311) diffraction planes of Au.

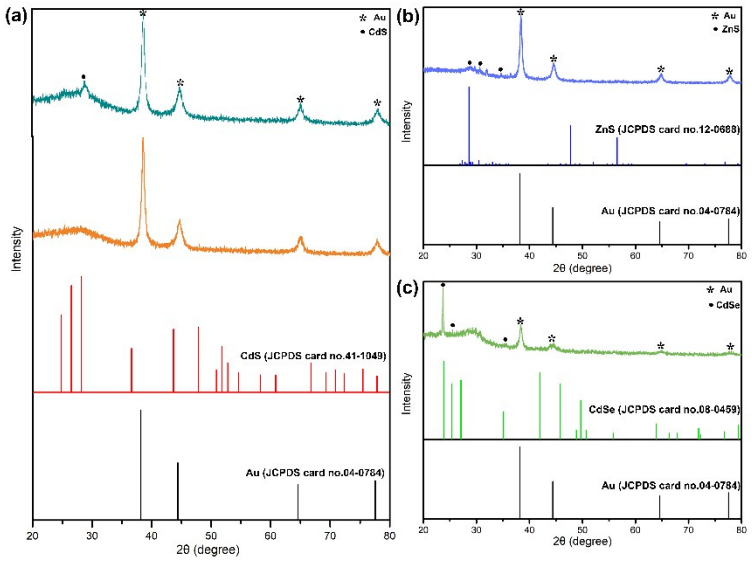

Figure S7. XRD patterns of Au@CdS NPs with 5 min (yellow line) and 8 min (green line) deposition (a), Au@ZnS (b) and Au@CdSe (c) NPs and PDF cards of the Au, CdS, ZnS and CdSe.

S6. TEM and SEM characterizations of Au@ZnS NPs.

Based on the potentiostatic deposition at -0.8 V *vs.* Pt for 5 and 10 min, ZnS was formed as shell on the surface of 40 nm AuNPs with highly uniform thickness, which was increased as time elapsed (Figure S8). The core-shell feature and crystalline form was further characterized by HRTEM and elemental mapping (Figure S9).

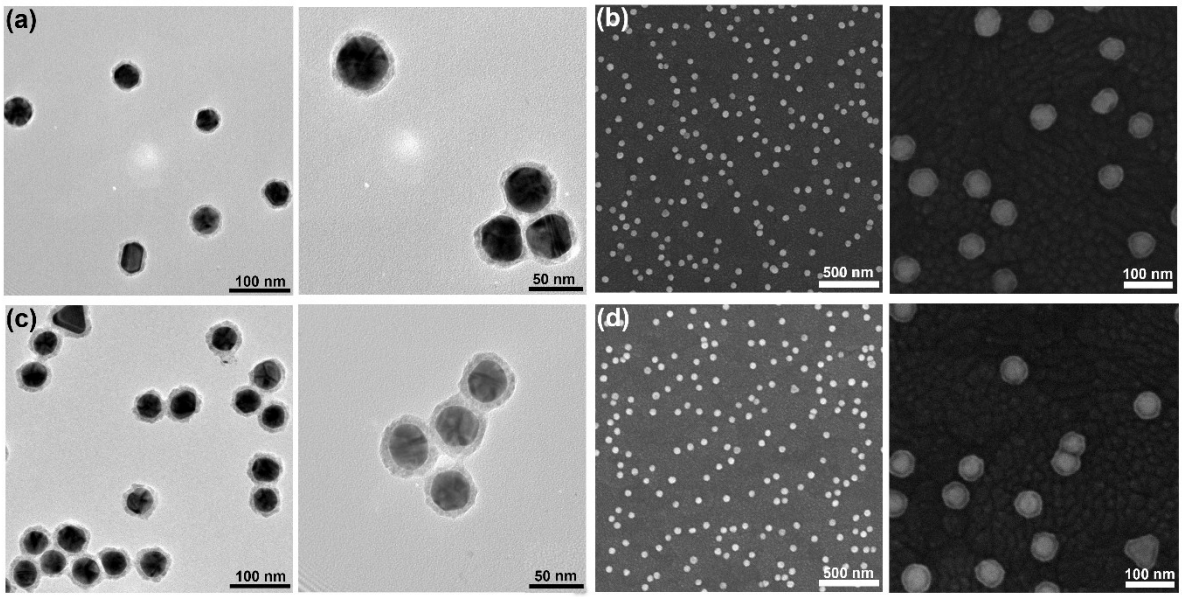

Figure S8. (a) (b). TEM (a, c) and SEM (b, d) images of AuNPs with application of -0.8 V for 5 and 10 min to form Au@ZnS NPs.

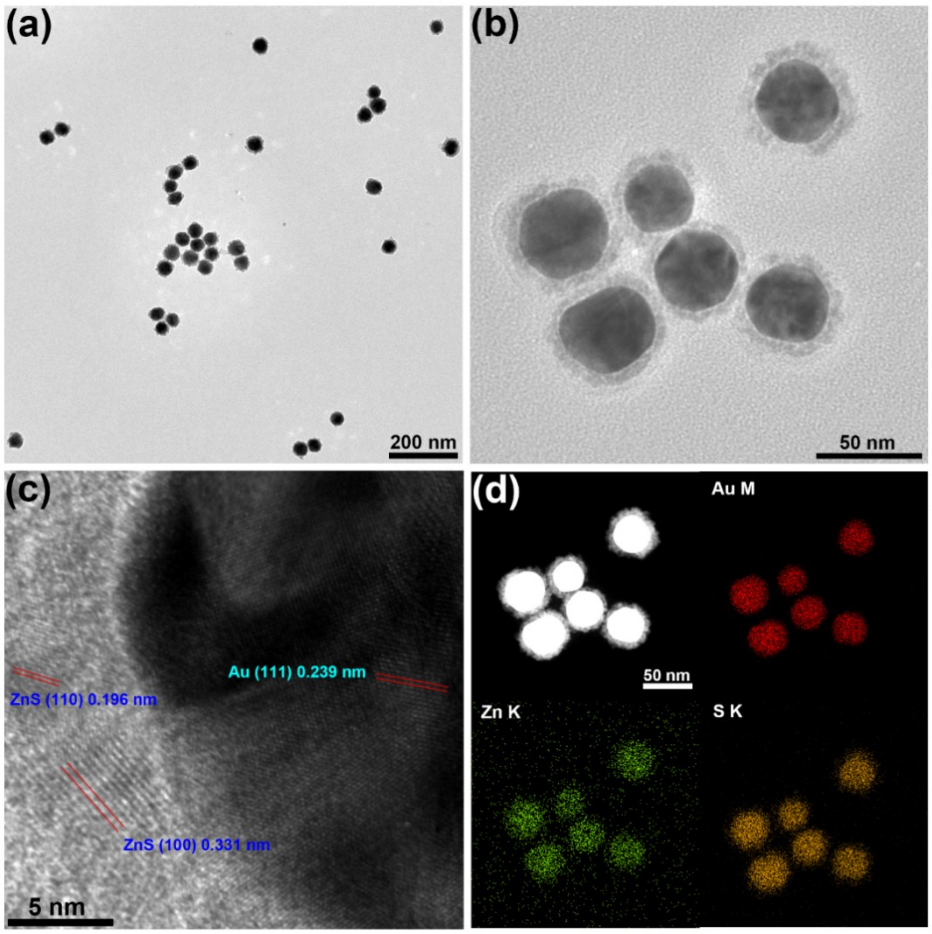

Figure S9. (a) (b) TEM images of Au@ZnS NPs. (c) HR-TEM images of Au@ZnS NPs. (d) EDX elemental mapping of the Au@ZnS NPs.

S7. TEM characterization of Au@CdSe NPs.

The nucleation and growth rates of CdSe were fast. Cyclic voltammetry sweeping from -0.4 V to -0.8 V (*vs.* Ag/AgCl) with scan rate of 100 mV/s for one cycle resulted in the formation of hexagonal CdSe on Au with shell thickness of 5 ± 2 nm (Figure S10). The core-shell feature and crystalline form was further characterized by HRTEM and elemental mapping.

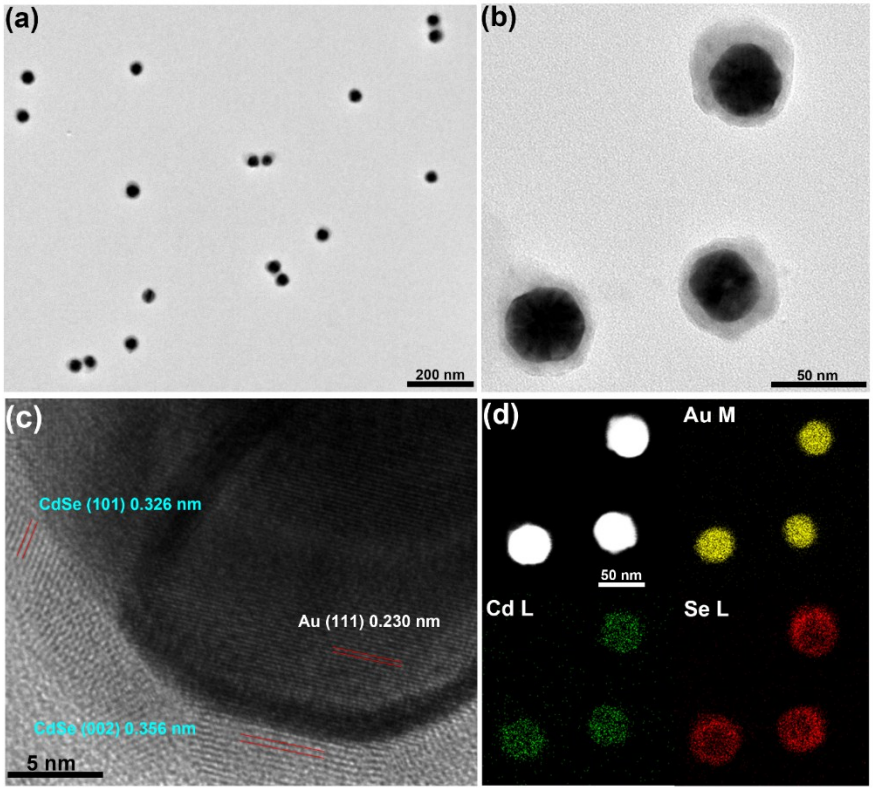

Figure S10. (a) (b) TEM images of Au@CdSe NPs. (c) HR-TEM images of Au@CdSe NPs. (d) EDX elemental mapping of the Au@CdSe NPs.

S8. Photocurrent responses of CdS and Au@CdS modified ITO electrodes.

The synthesis of CdS NPs on ITO is similar to that of Au@CdS NPs. The electrochemical deposition was performed using unmodified ITO working electrodes in pH 3.0 H_2SO_4 solution containing 0.1 M $CdCl_2$ and 10 mM $Na_2S_2O_3$ at room temperature. Unlike selective deposition on AuNPs *via* Au-S bond induced nucleation. CdS NPs with average diameter of 33 nm could be directly formed on ITO with longer deposition time (10 min). Compared to the photocurrent generation efficiencyiy of Au@CdS NPs on ITO with 2 min deposition time (48.4 μA cm^{-2}), that of CdS NPs on ITO under 532 nm laser irradiation is neglectable (Figure S11).

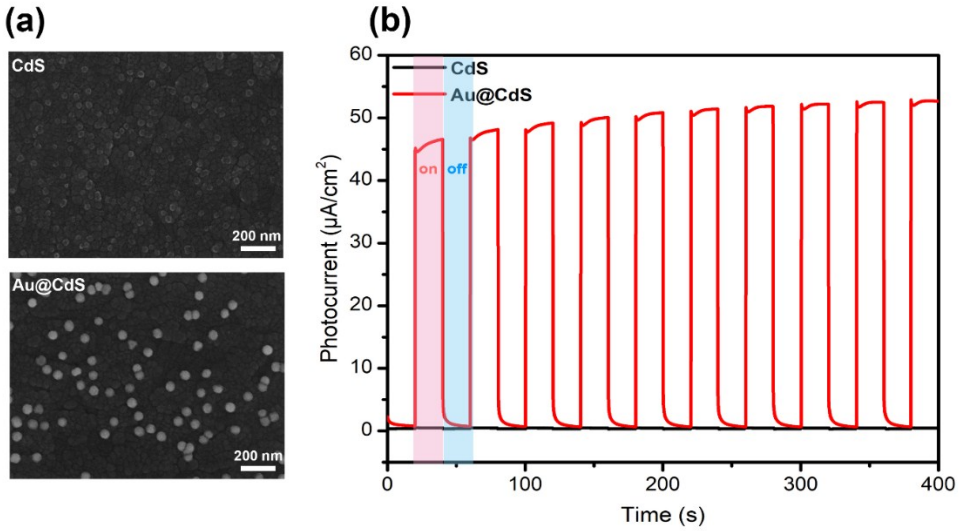

Figure S11. (a) SEM images of CdS NPs and Au@CdS NPs modified ITO electrodes. (b) Photocurrent of CdS NPs and Au@CdS NPs modified ITOs irradiated with visible light of 532 nm at -0.3 V (*vs.* SCE).

S9. Reference.

1. (a) T. Hirakawa and P. V. Kamat, *J. Am. Chem. Soc*., 2005, **127**, 3928-3934. (b) H. Rajbongshi, S. Bhattacharjee and P. Datta, *Materials Research Express*, 2017, **4**, 025501.